Wideband Type-II GaInAsSb/InP Uni-Traveling Carrier Photodiodes for Near 300 Gbps Communications

Rimjhim Chaudhary, Akshay M. Arabhavi, Laurenz Kulmer, Sara Hamzeloui, Martin Leich, Olivier Ostinelli, Juerg Leuthold, *Fellow, IEEE*, and Colombo R. Bolognesi, *Fellow, IEEE*

***Abstract*—We report the wideband performance of uniform Type-II GaInAsSb/InP UTC-PDs for optical data communications near 300 Gbps. A wide bandwidth of >110 GHz is achieved for a device area of 50 μm^2. In signal transmission measurements, the present UTC-PDs show a low Bit-Error Rate (BER) and a high Signal-to-Noise Ratio (SNR) of more than 18 dB at data rates as high as 288 Gbps (96 GBd, PAM-8) without post-amplification electronics. The work demonstrates the suitability of GaInAsSb/InP UTC-PDs for optical data transmission at bit rates approaching 300 Gbps.**

***Index Terms*—Uni-Traveling Carrier Photodiodes (UTC-PDs), high-bandwidth, high-power, eye-diagram, 300 Gbps, InP, GaInAsSb, optical communications.**

I. Introduction

INTEREST in Millimeter (MMW) and Terahertz (THz) waves for broadband communications grows to meet the demand for higher data rates. The bit rate for wireless communications in the marketplace is soon expected to reach 100 Gbps [1]. High rate transmission is also of interest to short-reach links used in data-center communications where cost and power consumption are major considerations. High-rate solutions often use several multiplexed lower-rate channels requiring much overhead in terms of electronics and signal processing [2], [3]. A single-photodiode 110 GHz Kramers-Kronig receiver achieved an impressive 400 Gbps [4]. 320 Gbps demultiplexing of a return-to-zero (RZ) data stream was also demonstrated by integrating a semiconductor-optical amplifier Mach-Zehnder interferometer (SOA-MZI) with a 160 GHz bandwidth back-illuminated 50 μm^2 UTC-PD in a 15 Ω system [5]. The present work demonstrates near 300 Gbps detection into a 50 Ω load with a compact low-cost top-illuminated GaInAsSb/InP UTC-PD.

In the THz frequency range (100 GHz to 10 THz), all-electronic transistor-based technologies still face the arduous task of realizing broadband THz generator circuits due to the difficulties in realizing solid-state signal sources in the so-called "THz-gap". On the other hand, photonics are an excellent alternative to conventional electronic systems for generating signals in the MMW and THz range [6]. Optical beat generators are better suited for continuous-wave low phase noise sources and are much easier to build in terms of stability and system configuration. Moreover, optical fibers enable high-frequency signal distribution over long distances without lossy metallic transmission media such as coaxial cables or bulky hollow waveguides. An optical-to-electrical (O/E) signal interface using high-bandwidth photodiodes is a critical component of such systems. Additionally, the high-power capability of a photodiode is crucial, as it eliminates the need for high-bandwidth post-amplification electronics, thus extending the bandwidth of the entire system [7].

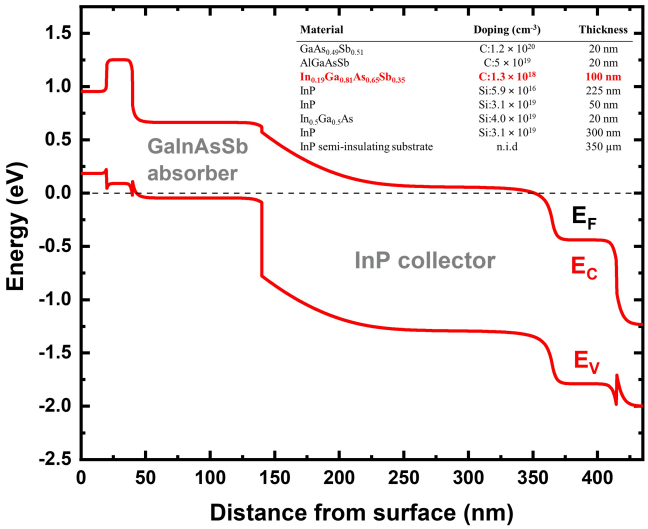

Fig. 1. Simulated equilibrium band diagrams of the Type-II GaInAsSb UTC-PD. Fermi level is shown as E_F = 0 eV. (*Inset*: Corresponding epitaxial layer structure.)

Uni-traveling carrier photodiodes (UTC-PDs), primarily involving only the transport of fast-moving carriers (electrons), exhibit higher bandwidths and superior power responses than conventional PIN photodiodes. Their high linearity and high saturation current provide the necessary signal power at high frequencies without requiring post-amplification. UTC-PDs have been reported with bandwidths of 310 GHz and high saturation currents of 27 mA, with an output power of 10 dBm at 100 GHz, which prove advantageous for high bit-rate applications [8]–[10].

We previously demonstrated "Type-II" GaInAsSb/InP UTC-

R. Chaudhary, A. M. Arabhavi, S. Hamzeloui, M. Leich, O. Ostinelli, and C. R. Bolognesi are with the Millimeterwave Electronics (MWE) group at the Department of Information and Technology, ETH Zürich, 8092 Zürich, Switzerland *(Corresponding Author: C. R. Bolognesi, colombo@ieee.org).*

L. Kulmer and J. Leuthold are with the Institute of Electromagnetic Fields (IEF) at the Department of Information and Technology, ETH Zürich, 8092 Zürich, Switzerland

Manuscript received April 19, 2005; revised August 26, 2015.

PDs with improved electron transport properties compared to GaInAs/InP and GaAsSb/InP UTC-PDs [11]–[13]. $GaAs_{0.51}Sb_{0.49}$ grown lattice-matched to InP displays a relatively low electron mobility because of its low Γ-L valley separation ($\Delta_{\Gamma\text{-L}} \approx 90$ meV) [14]. Alloying In- to GaAsSb raises the L- satellite valley relative to GaAsSb and reduces the electron population of the low-mobility L-valleys. This improves both the electron mobility and the transit time limited bandwidth of GaInAsSb/InP UTC-PDs [14], [15], since the L-valley forms a "Type-I" blocking barrier with the InP collector. The simple grading-free epitaxial structure with a pure InP collector enables reproducible growth and fabrication, leading to a low-cost and stable device process.

In the present work, we characterized Type-II GaInAsSb-based UTC-PDs up to 110 GHz and performed optical data transmission measurements up to 288 Gbps. We developed a small-signal equivalent circuit that accurately models the transfer and optical behavior of the PDs. Our top-illuminated UTC-PDs show a bandwidth exceeding 110 GHz for a 50 μm^2 device area and of 110 GHz for 64 μm^2 device area. In both cases the responsivity is 0.1 A/W. In data transmission experiments our UTC-PDs achieve a low Bit-Error Rate (BER) of 2.75×10^{-2} and a high SNR of more than 18 dB for data rates up to 288 Gbps (96 GBd, PAM-8) without any post-amplification electronics. These results demonstrate the suitability of GaInAsSb as an advanced absorber for UTC-PDs in optical data transmission, supporting bit rates up to 300 Gbps.

II. EPITAXIAL STRUCTURE AND DEVICE FABRICATION

The simulated equilibrium band diagram showing the Type-II band alignment of GaInAsSb UTC-PD is shown in Fig. 1. The design includes a 225 nm n-type InP collector doped at 5.9×10^{16} cm^{-3} and a p-type 100 nm uniform quaternary $Ga_{0.81}In_{0.19}As_{0.65}Sb_{0.35}$ absorber doped at 1.36×10^{18} cm^{-3}. The epitaxial layers detailed in the inset of Fig. 1 were grown by Metal-Organic Vapor-Phase Epitaxy (MOVPE) on a 2-inch semi-insulating (100) InP substrate at ETH Zürich.

Photodiodes of varying areas were fabricated by successive optical lithography and wet etching steps [11], followed by a low-temperature (≤ 190°C) Teflon-based etch-back planarization process for co-planar waveguide (CPW) probe pad deposition [16]. Fig. 2 shows the top view optical microscope image of a completed UTC-PD.

III. RESULTS AND DISCUSSION

A. DC and High-Frequency Response

DC characterization of the UTC-PDs was performed using an HP 4156B semiconductor parameter analyzer. The room temperature *I-V* characteristics show a dark current of less than 10 nA up to a reverse bias of 5 V, as shown in Fig. 2. The measured responsivity of a top-illuminated photodiode peaks at 0.1 A/W at 1550 nm. The device responsivity is independent of polarization and compares well to the Ito *et al.*, with a two-pass (back-illuminated with topside reflector) GaInAs absorber

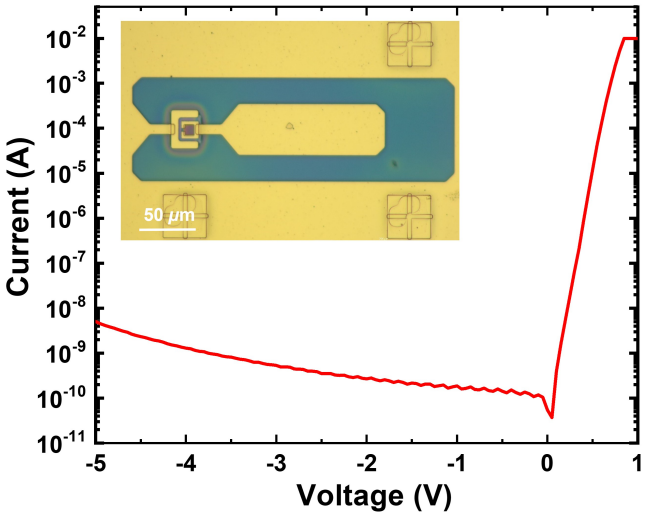

Fig. 2. *I-V* characteristics of a 50 μm^2 device size, showing low dark current. (*Inset*: Top-view microscopic image of a fabricated UTC-PD with the co-planar waveguide probe pads.)

[8]. Our device responsivity can be improved by the use of DBR back mirrors as was shown in [17]. It is important to note that the UTC-PDs' low responsivity isn't a major issue, as optical inputs can be amplified using an optical amplifier. Instead high bandwidth and high linearity of UTCs are crucial for strong RF power and reliable signal transmission.

Two distinct characterization setups were employed to cover a broad range of measurement frequencies. In both cases, devices were tested with a 50 Ω load. First, the normalized frequency response up to 67 GHz was measured using a Thorlabs MX70G lithium niobate ($LiNbO_3$) Mach-Zehnder modulator (MZM) electrical-to-optical (E/O) converter at λ = 1550 nm and a PNA-X vector network analyzer. Fig. 3 shows the schematic of the RF measurement setup. A Line/Reflect/Match (LRM) coaxial calibration technique was employed using the E-Cal module N4694-60001, up to 67 GHz. The RF probe at port 2 was then de-embedded to bring the reference plane to the probe tip on the output port and at the end of the RF cable at the input port. The modulator's frequency response was later de-embedded as per [18] to extract the RF response of the devices.

For higher-frequency measurements from 75 to 110 GHz, a two-tone optical heterodyne system at λ = 1550 nm was used to generate the RF signal by the superposition of two equal amplitude lasers with a controllable frequency offset. Fig. 3 shows the schematic of the measurement setup with the two lasers. The frequency offset can be controlled by tuning one laser frequency with respect to the second. Both lasers were combined with a 3-dB coupler and then guided through the optical fiber onto the photodiode. A W-band RF probing system and an HP 8486A W-band RF power meter were used to measure the output response of the UTC-PDs. The RF power reported here was carefully de-embedded, considering a maximum insertion loss of about 1.3 dB of the WR-10 waveguide probes. For both setups, the modulated light signal was amplified using an Erbium-Doped Fiber Amplifier (EDFA) and coupled onto the top-illuminated PDs using a single-

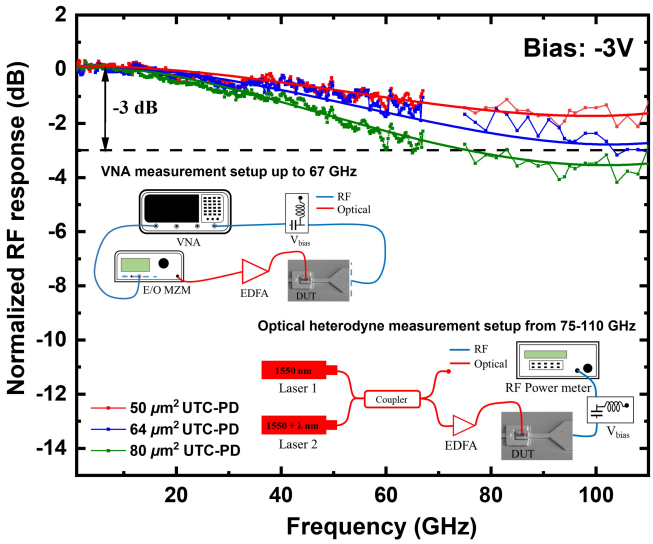

Fig. 3. Measured and equivalent circuit model fitted (bold lines) frequency response of UTC-PDs for sizes ranging from 50 to 80 μm^2. The two different RF measurement set-ups are also shown in the picture.

mode optical fiber with a spot diameter of $\sim 9\,\mu$m. Fig. 3 shows the measured and simulated (detailed later) normalized frequency response plotted with frequency for UTC-PDs of different areas at a reverse-bias of 3 V to ensure full depletion of the collector and a photocurrent of 1 mA. To normalize the frequency response, two-tone measurements were also conducted in the frequency range of 2-50 GHz. The data from these two measurement setups were then overlapped to obtain the final frequency response. A flat frequency response was measured up to 110 GHz for a device size of 50 μm^2 showing the $f_{3\text{dB}}$ cutoff exceeding 110 GHz. For 64 and 80 μm^2 devices, the $f_{3\text{dB}}$ cutoff was 110 and 80 GHz, respectively. The high-power and high-saturation performance of these devices at high frequencies was previously reported in [13].

B. 110 GHz Small-Signal Equivalent Circuit

The measured RF response of the UTC-PDs shows flattening of the roll-off at frequencies $\geq$ 85 GHz. To clarify this observation, S_{22} is measured up to 110 GHz after a line-reflect-reflect-match (LRRM) calibration to bring the reference plane to the probe tip. Next, the Keysight Advanced Design System (ADS) gradient optimizer was used to fit the circuit model to the measurement data. The model was designed to minimize the error goals defined as the difference between the measured and modeled phase of S_{22} and the measured RF response and modeled S_{21} of the UTC-PD up to 110 GHz. Fig. 4 (a) shows the two-port equivalent small-signal circuit used to model the UTC-PDs, along with the CPW pads. We previously reported an equivalent circuit model of our UTC-PDs, showing a resistive and capacitive behavior of the devices up to 67 GHz. The CPW pads are designed so that the elements of the equivalent circuits of the OPEN and SHORT test structures are independent of the frequency up to 67 GHz and, thus, do not affect the normalized RF device response below 67 GHz [19]. However, for higher frequencies, the

TABLE I
EQUIVALENT CIRCUIT ELEMENTS FOR DIFFERENT SIZES

Equivalent Circuit Element:	50 μm^2	64 μm^2	80 μm^2
C_j – Diode junction capacitance (fF):	21	25	33
R_s – Diode series resistance (Ω):	5.5	5.5	5.5
C_{ab} – Pad airbridge capacitance (fF):	17	17	17
L_{ab} – Pad airbridge inductance (pH):	40	40	40
C_a– Pad access capacitance (fF):	20	20	20
L_a – Pad access inductance (pH):	7.5	7.5	7.5
C_{pad} – Pad capacitance (fF):	0.1	0.1	0.1
L_{pad} – Pad inductance (pH):	6	6	6
R_{pad} – Pad series resistance (Ω):	4.3	4.3	4.3
f_{RC} – RC limited cutoff (GHz):	156	150	88

impact of parasitic interconnects effects becomes noticeable and should be accounted for in the equivalent circuit model. A part of the updated small-signal equivalent circuit in Fig. 4 (a) is superimposed on the FIB/SEM image of the fabricated UTC-PDs in Fig. 4 (b) to indicate the physical association between model elements and the device structure. R_τ and C_τ at the input port mimic the frequency response roll-off due to the transit time delay of the PDs, whereas the circuit element at the output port determines the RC-limited roll-off. The intrinsic device is represented by a junction capacitance, C_j, describing the absorber-collector junction, and a series resistance, R_s, representing the bulk resistance contribution of the bulk absorber, as well as the collector and absorber contact resistances. In parallel to the junction capacitance, the transconductance of the voltage-controlled-current-source (VCCS) is used to tune the absolute response (power) level for different device sizes. To model the behavior of the pad parasitics up to 110 GHz, three different LC sections were added to the circuit model, as shown in Fig. 4 (b) [19]. The first section, L_{ab} and C_{ab}, represents the parasitic behavior of the mesa bridge with Teflon underneath. The second section, L_a and C_a, represents the access parasitic caused by the tapering of the pads near the device, and the last section, L_{pad}, and C_{pad}, represents the pad parasitic of the GSG pads. Finally, R_{pad} represents the resistances of the metal contacts.

On completion of the measurements, both measured and fitted photoresponses are normalized to the near DC (0.2 GHz) value to obtain the normalized response curves plotted in Fig. 3. At frequencies higher than 85 GHz, the devices show an inductive coupling of the pads, resulting in the flattening of the device RF response [20]. Fig. 4 (c) shows the measured and fitted S_{22} on the Smith chart for different-sized devices, demonstrating an excellent agreement with the measured data. The fitted values for equivalent circuit elements of different device sizes are given in Table I.

The measured 3-dB cutoff frequency ($f_{3\text{dB}}$) of a PD is determined by the transit time limited bandwidth (f_τ) and the RC-limited bandwidth, (f_{RC}) as:

$$\frac{1}{f_{3dB}^2} = \frac{1}{f_{RC}^2} + \frac{1}{f_\tau^2} = (2\pi RC)^2 + \frac{1}{f_\tau^2}$$

where, R is the sum of PD series resistance and the load resistance of 50 Ω, and C is the PD capacitance inclusive

TABLE II
COMPARISON OF DIFFERENT UTC TECHNOLOGIES

Ref.	Absorber	Collector	Technology	Area (μm^2)	f_{3dB} (GHz)	Responsivity (A/W)
[9]	220 nm GaInAs (Uniform)	263 nm InP	Back-illuminated	52	65*	0.3
[22]	120 nm GaInAs (Uniform)	300 nm InP	Waveguide	45	90	0.35
[23]	200 nm GaInAs (Graded)	300 nm GaInAsP	Waveguide	40	80	0.25
[24]	160 nm GaInAs (Graded)	250 nm InP	Flip-chip bonded	50	90	0.15
[25]	90 nm GaAsSb/ 70 nm GaInAs (Graded)	100 nm InP	Flip-chip bonded	50	60	0.11
[26]	100 nm GaAsSb (Graded)	250 nm InP	Back-illuminated	38	100	0.11
This work	**100 nm GaInAsSb (Uniform)**	**225 nm InP**	**Top-illuminated**	**50**	**>110**	**0.1**
This work	**100 nm GaInAsSb (Uniform)**	**225 nm InP**	**Top-illuminated**	**64**	**110**	**0.1**

*Measured with a load resistance of 25 Ω

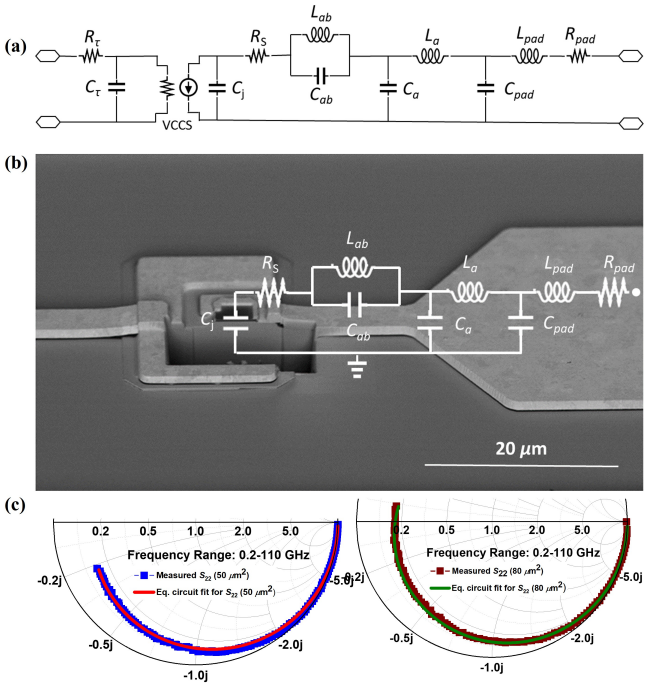

Fig. 4. (a) Equivalent circuit model used to fit the measured response of the UTC-PDs. (b) FIB/SEM cross-section of the fabricated UTC-PDs with the superimposed small signal equivalent circuit model. (c) Measured and fitted S_{22} vs. frequency of UTC-PDs for two different sizes between 0.2-110 GHz.

of the junction capacitance at a given bias and the parasitic capacitance. The transit time-limited cut-off frequency of a 100 nm GaInAsSb-based absorber has previously been demonstrated to be around 274 GHz [11]. The devices exhibit RC-limited behavior and have significant scope for improving the overall bandwidth by scaling the area. Table II compares the present performances with published results for UTC-PDs of similar sizes. Although the present devices are RC-limited, uniform GaInAsSb based UTC-PDs exhibit superior overall bandwidth in comparison to the graded GaInAs and GaAsSb-based UTC-PDs [11]. This performance advantage can be attributed to the enhanced transport properties of GaInAsSb and a thinner absorber. Further enhancement of the transit-time limited cutoff can in principle be achieved through the use of composition and/or doping grading schemes in the absorber.

C. 288 Gbps Optical Transmission Measurements

To asses the potential of our UTC-PDs for high-speed optical data communications, we performed eye diagram measurements using Pulse Amplitude Modulation (PAM) signaling (PAM-2/4/8). The experimental setup depicted in Fig. 5 (a) relied on a 128 GSa/s arbitrary waveform generator (AWG) to generate pre-amplified random bit sequences, which were then fed to a Thorlabs MX70G electrical-to-optical modulator. The signal was amplified by an EDFA up to 18 dBm and transmitted via an optical fiber to the photodetector. The device was measured at a photocurrent of 7 mA and was reverse-biased at 3 V through a bias-tee. The generated electrical signal from the UTC-PD was then read out through the WR-10 waveguide GSG probes by a digital sampling oscilloscope (DSO) without any post-amplification of the RF signal. The high output power of the UTC-PDs, attributed to the device's high linearity, provided the necessary signal power to perform experiments at such high frequencies. Finally, common offline digital signal processing (DSP) techniques were applied, including timing recovery, a least mean square (LMS) equalization, and a nonlinear pattern-dependent equalization. This was followed by a second LMS equalization and symbol decision to evaluate the bit-error rates (BER) and signal-to-noise ratio (SNR). Figs. 5 (b)-(e) show the detected electrical eye-diagrams for 64 - 288 Gbps signals with PAM-2, PAM-4, and PAM-8 modulation using an NRZ pulse shape. The BER for up to 192 Gbps with PAM-4 and 128 Gbps with PAM-2 modulation is below the hard decision forward-error-correction (HD-FEC) limit of 3.8×10^{-3}. Similarly, the BER for 256 Gbps with PAM-4 , as well as the 288 Gbps PAM-8, modulated signal remains below the soft decision forward-error-correction (SD-FEC) limit of 4.2×10^{-2} [21]. The maximum achievable bit rate is limited by the measurement equipment (including the modulator used in the experiment, which has a frequency limit of 70 GHz). High SNR values ranging from 13 to 19 dB were obtained for the specified data rates. The SNR encompasses

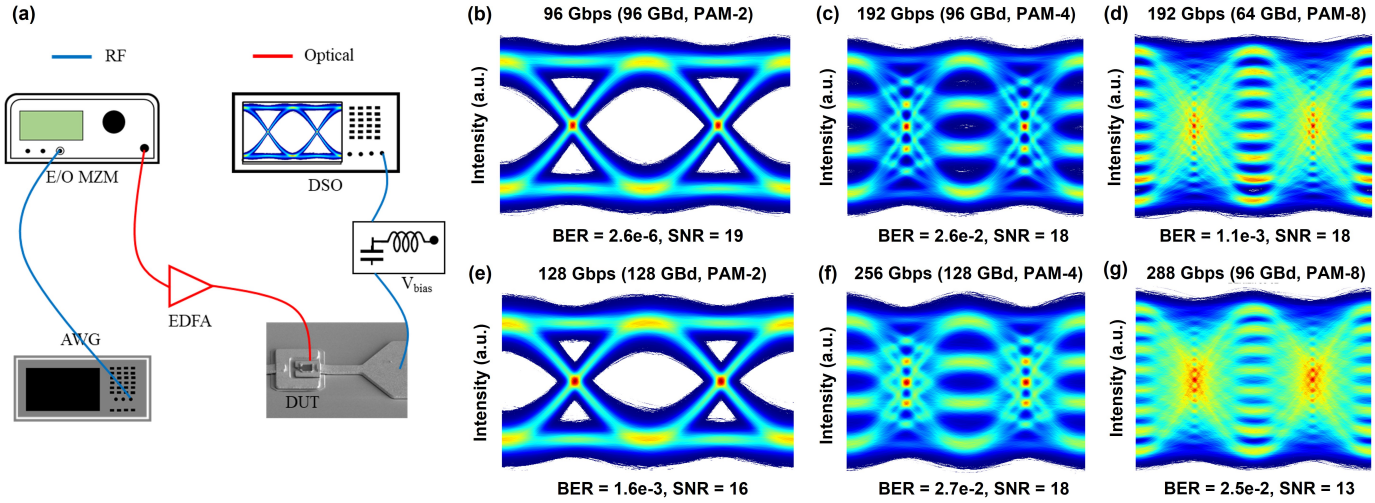

Fig. 5. (a) Schematic of the measurement setup used for the eye-diagram measurements. Detected eye diagrams of (b) 96 Gbps (96 GBd, PAM-2), (c) 192 Gbps (96 GBd, PAM-4), (d) 192 Gbps (64 GBd, PAM-8), (e) 128 Gbps (128 GBd, PAM-2), (f) 256 Gbps (128 GBd, PAM-4), and (g) 288 Gbps (96 GBd, PAM-8) for a 64 μm^2 device size. The bit-error-rate (BER) and the Signal-to-Noise Ratio (SNR) are also indicated.

noise from the overall system, including the transmitter, the optical amplifiers, and the receiver. The eye diagram noise likely is dominated by contributions from the test set-up including interconnects and notably the 70 GHz modulator used for measurements, these make it impossible to extract the UTC-PD noise contributions at this time. The present results indicate that the data experiment is not intrinsically limited by the detector performance, but rather by the overall test set-up.

IV. Conclusion

We have extensively characterized Type-II GaInAsSb-based UTC-PDs through RF and eye-diagram measurements. The Type-II band alignment of GaInAsSb with InP, combined with the improved electron mobility with respect to GaAsSb, make GaInAsSb an advantageous absorber material for UTC-PDs. A record f_{3dB} bandwidth exceeding 110 GHz was achieved for a device area of 50 μm^2. We developed an equivalent circuit model that fully reproduces measured characteristics response up to 110 GHz. In optical transmission experiments, the present UTC-PDs achieved detection up to 288 Gbps under PAM-8 signaling with a low BER and high SNR for a 64 μm^2 device area without post-amplification. The results demonstrate potential for next-generation optical and microwave photonic communication at bit rates approaching 300 Gbps with minor device modifications. Reducing the active device area and the implementation of a graded GaInAsSb absorber are expected to further enhance the overall bandwidth of the UTC-PDs. The present study highlights the interest in GaInAsSb absorbers in UTC-PDs using simple, easily manufacturable top-illuminated structures for optical communication applications. Future work will focus on improving the overall responsivity with resonant cavity structures. Significant improvements in responsivity are expected since optical electromagnetic simulations for the present UTC-PD show that the peak optical field region is not aligned with the absorber layers.

Acknowledgment

The authors would like to thank the staff of FIRST Lab at ETH Zurich, Zurich, Switzerland, for their support.

References

[1] IEEE standard for high data rate wireless multi-media networks–amendment 2: 100 Gb/s wireless switched point-to-point physical layer, in IEEE standard 802.15.3d-2017 (amendment to IEEE Standard 802.15.3-2016 as amended by IEEE standard 802.15.3e-2017), 18 October 2017, pp. 1–55.

[2] F. E. Doany *et al.*, "300-Gb/s 24-channel bidirectional Si carrier transceiver Optochip for board-level interconnects," *2008 58th Electronic Components and Technology Conference*, Lake Buena Vista, FL, USA, 2008, pp. 238-243, doi: 10.1109/ECTC.2008.4549976

[3] J. Zhang *et al.*, "Demonstration of Single-Lane 350-Gb/s PS-PAM-16 in the C-band using single-DAC for Data Center Interconnects," *2021 Optical Fiber Communications Conference and Exhibition (OFC)*, San Francisco, CA, USA, 2021, pp. 1-3. Th5F.4

[4] I. Sackey *et al.*, "Distributed Aggregation and Reception of a 400-Gb/s Net Rate Superchannel in a Single-Photodiode 110-GHz Kramers-Kronig Receiver," *2018 Optical Fiber Communications Conference and Exposition (OFC)*, San Diego, CA, USA, 2018, pp. 1-3. Th4C.7

[5] S. Kodama, T. Yoshimatsu and H. Ito, "320-Gbit/s Demultiplexing with Monolithic PD-EAM Optical Gate," *2002 28TH European Conference on Optical Communication (ECOC)*, Copenhagen, Denmark, 2002, pp. 1-2.

[6] T. Nagatsuma, G. Ducournau, and C. Renaud, "Advances in terahertz communications accelerated by photonics," *Nature Photon.* vol. 10, no. 6, pp. 371– 379, 2016, doi: 10.1038/nphoton.2016.65

[7] T. Ishibashi, Y. Muramoto, T. Yoshimatsu, and H. Ito, "Unitraveling-Carrier Photodiodes for Terahertz Applications," in *IEEE J. Sel. Top. Quantum Electron.*, vol. 20, no. 6, pp. 79-88, Nov.-Dec. 2014, Art no. 3804210, doi: 10.1109/JSTQE.2014.2336537.

[8] H. Ito, T. Furuta, S. Kodama, and T. Ishibashi, "InP/InGaAs unitravelling-carrier photodiode with 310 GHz bandwidth," in *Electron. Lett.*, vol. 36, no. 21, pp. 1809-1810, Oct. 2000, doi: 10.1049/el:20001274.

[9] H. Ito, S. Kodama, Y. Muramoto, T. Furuta, T. Nagatsuma, and T. Ishibashi, "High-speed and high-output InP-InGaAs unitraveling-carrier photodiodes," in *IEEE J. Sel. Top. Quantum Electron.*, vol. 10, no. 4, pp. 709-727, July-Aug. 2004, doi: 10.1109/JSTQE.2004.833883.

[10] V.K. Chinni, *et al.*, "Single-channel 100 Gbit/s transmission using III–V UTC-PDs for future IEEE 802.15.3d wireless links in the 300 GHz band," in *Electron. Lett.*, vol. 54, no. 10, pp. 638-640, 2018, doi: 10.1049/el.2018.0905

[11] A. M. Arabhavi *et al.*, "Type-II GaInAsSb/InP Uniform Absorber High Speed Uni-Traveling Carrier Photodiodes," in *J. Light. Technol.*, vol. 39, no. 7, pp. 2171-2176, Apr. 2021, doi: 10.1109/JLT.2020.3043537

[12] R. Chaudhary, O. Ostinelli, A. M. Arabhavi, and C. R. Bolognesi, "Bias-Free Operation of Type-II GaInAsSb/InP High-Speed Uni-Traveling Carrier Photodiodes," *2022 IEEE Photonics Conference (IPC)*, Vancouver, BC, Canada, 2022, pp. 1-2, doi: 10.1109/IPC53466.2022.9975445.

[13] R. Chaudhary *et al.*, "High-Power Performance of Type-II GaInAsSb/InP Uniform Absorber Uni-Traveling Carrier Photodiodes," in *2023 Optical Fiber Communications Conference and Exhibition (OFC)*, San Diego, CA, USA, 2023, pp. 1-3.Th2A.7.

[14] C. R. Bolognesi and O. J. S. Ostinelli, "Γ-L intervalley separation and electron mobility in GaAsSb grown on InP: Transport comparison with the GaInAs and GaInAsSb alloys," in *Appl. Phys. Lett.*, vol. 119, no. 24, pp. 242103, Dec. 2021, doi: 10.3929/ethz-b-000522371

[15] W. Quan, A. M. Arabhavi, R. Flückiger, O. Ostinelli, and C. R. Bolognesi, "Quaternary graded-base InP/GaAsSb DHBTs with f_T/f_{MAX} =547/784 GHz," in *IEEE Electron Device Lett.*, vol. 39, no. 8, pp. 1141–1144, Aug. 2018, doi: 10.1109/LED.2018.2849351.

[16] R. Flückiger, R. Lövblom, O. Ostinelli, H. Benedickter, and C. R. Bolognesi, "InP/GaAsSb DHBTs fabricated in a low-temperature teflon planarization process," in *IEEE Electron Device Lett.*, vol. 33, no. 8, pp. 1135–1137, Aug. 2012, doi: 10.1109/LED.2012.2201443.

[17] R. Chaudhary, A. M. Arabhavi, O. Ostinelli, M. Leich and C. R. Bolognesi, "Type-II GaInAsSb Based Uni-traveling Carrier Photodiodes with AlGaInAs/InP Bragg Reflectors for Improved 1.55 μm Responsivity", in *6th International Conference on Optics, Photonics and Lasers (OPAL' 2023)*, Funchal (Madeira Island), Portugal, May, 2023.

[18] "De-embed application note for Thorlabs MX40/70G calibrated electrical-to-optical converter," May 16, 2017. [Online]. Available:https://www.thorlabs.com/drawings/b165527791896268-8FE28E97-D159-37BB-FF990460EBBF3742/MX70G-De-EmbedApplicationNote.pdf

[19] D. Guendouz, *et al.*, "Multiscale Compact Modelling of UTC-Photodiodes Enabling Monolithic Terahertz Communication Systems Design." in *Appl. Sci.*, vol. 11, no. 23, pp. 11088, 2021 doi: 10.3390/app112311088

[20] A. Novack, *et al.*, "Germanium photodetector with 60 GHz bandwidth using inductive gain peaking," in *Opt. Express*, Vol. 21, no. 23, pp. 28387-28393, Nov. 2013, doi: 10.1364/OE.21.028387

[21] Q. Hu *et al.*, "Ultrahigh-Net-Bitrate 363 Gbit/s PAM-8 and 279 Gbit/s Polybinary Optical Transmission Using Plasmonic Mach-Zehnder Modulator," in *J. Light. Technol.*, vol. 40, no. 10, pp. 3338-3346, May 2022, doi: 10.1109/JLT.2022.3172246.

[22] E. Rouvalis *et al.*, "High-speed photodiodes for InP-based photonic integrated circuits," in *Opt. Express*, vol. 20, no. 8, pp. 9172-9177, Apr. 2012, doi: 10.1364/OE.20.009172

[23] M. Anagnosti *et al.*, "Optimized High Speed UTC Photodiode for 100 Gbit/s Applications," in *IEEE J. Sel. Top. Quantum Electron.*, vol. 20, no. 6, pp. 29-35, Nov.-Dec. 2014, doi: 10.1109/JSTQE.2014.2316594.

[24] C. Wei *et al.*, ">110 GHz High-Power Photodiode by Flip-Chip Bonding," in *2022 IEEE International Topical Meeting on Microwave Photonics (MWP)*, Orlando, FL, USA, 2022, pp. 1-4, doi: 10.1109/MWP54208.2022.9997642.

[25] J. M. Wun, Y. W. Wang and J. W. Shi, "Ultrafast Uni-Traveling Carrier Photodiodes With $GaAs_{0.5}Sb_{0.5}/In_{0.53}Ga_{0.47}As$ Type-II Hybrid Absorbers for High-Power Operation at THz Frequencies," in *IEEE J. Sel. Top. Quantum Electron.*, vol. 24, no. 2, pp. 1-7, Mar.-Apr. 2018, doi: 10.1109/JSTQE.2017.2741106.

[26] J. S. Morgan *et al.*, "Bias-Insensitive GaAsSb/InP CC-MUTC Photodiodes for Mmwave Generation up to 325 GHz," in *J. Light. Technol.*, doi: 10.1109/JLT.2023.3298772.